tinctive features are very similar to those observed in the ~2500-Ma Mt. McRae Shale, and their age is supported by more thorough analytical protocols (*24*). The discovery and careful analysis of biomarkers in rocks of still greater age and of different Archean environments will potentially offer new insights into early microbial life and its evolution.

References and Notes

1. J. W. Schopf, *Science* **260**, 640 (1993).
2. M. R. Walter, in *Earth's Earliest Biosphere*, J. W. Schopf, Ed. (Princeton Univ. Press, Princeton, NJ, 1983), pp. 187–213.
3. S. J. Mojzsis *et al.*, *Nature* **384**, 55 (1996).
4. J. M. Hayes, I. R. Kaplan, K. W. Wedeking, in (*2*), pp. 93–134.
5. F. D. Mango, *Nature* **352**, 146 (1991).
6. A. Dutkiewicz, B. Rasmussen, R. Buick, *ibid.* **395**, 885 (1998).
7. K. E. Peters and J. M. Moldowan, *The Biomarker Guide* (Prentice-Hall, Englewood Cliffs, NJ, 1993).
8. R. C. Morris, *Precambrian Res.* **60**, 243 (1993).
9. A. F. Trendall, D. R. Nelson, J. R. de Laeter, S. W. Hassler, *Aust. J. Earth Sci.* **45**, 137 (1998).
10. N. T. Arndt, D. R. Nelson, W. Compston, A. F. Trendall, A. M. Thorne, *ibid.* **38**, 261 (1991).
11. R. E. Smith, J. L. Perdrix, T. C. Parks, *J. Petrol.* **23**, 75 (1982).
12. J. M. Gressier, thesis, University of Sydney, Sydney, Australia (1996).
13. T. C. Hoering and V. Navale, *Precambrian Res.* **34**, 247 (1987).
14. D. R. Nelson, A. F. Trendall, J. R. de Laeter, N. J. Grobler, I. R. Fletcher, *ibid.* **54**, 231 (1992).
15. R. E. Summons, T. G. Powell, C. J. Boreham, *Geochim. Cosmochim. Acta* **52**, 1747 (1988).
16. R. E. Summons and M. R. Walter, *Am. J. Sci.* **290A**, 212 (1990).
17. T. C. Hoering, *Carnegie Inst. Wash. Yearb.* **64**, 215 (1965); *ibid.* **65**, 365, (1966).
18. G. A. Logan, J. M. Hayes, G. B. Heishima, R. E. Summons, *Nature* **376**, 53 (1995); G. A. Logan, R. E. Summons, J. M. Hayes, *Geochim. Cosmochim. Acta* **61**, 5391 (1997).
19. G. A. Logan *et al.*, *Geochim. Cosmochim. Acta*, **63**, 1345 (1999).
20. S. J. Rowland, *Org. Geochem.* **15**, 9 (1990).
21. J. M. Hayes, in *Early Life on Earth*, Nobel Symposium No. 84, S. Bengtson, Ed. (Columbia Univ. Press, New York, 1994), pp. 220–236.
22. J. W. Schopf and B. M. Packer, *Science* **237**, 70 (1987).
23. R. Buick, *ibid.* **255**, 74 (1992).
24. R. E. Summons, L. L. Jahnke, J. M. Hope, G. A. Logan, *Nature*, in press.
25. H. D. Holland and N. J. Beukes, *Am. J. Sci.* **290A**, 1 (1990); A. H. Knoll and H. D. Holland, in *Effects of Past Global Change on Life*, S. M. Stanley, Ed. (National Academy Press, Washington, DC, 1995), pp. 21–33.
26. P. S. Braterman, A. G. Cairns-Smith, R. W. Sloper, *Nature* **303**, 163 (1983).
27. F. Widdel *et al.*, *ibid.* **362**, 834 (1993).
28. P. Cloud, *Science* **160**, 729 (1968); *Econ. Geol.* **68**, 1135 (1973).
29. G. Ourisson, M. Rohmer, K. Poralla, *Annu. Rev. Microbiol.* **41**, 301 (1987).
30. W. Kohl, A. Gloe, H. Reichenbach, *J. Gen. Microbiol.* **129**, 1629 (1983).
31. T.-M. Han and B. Runnegar, *Science* **257**, 232 (1992); A. H. Knoll, *ibid.* **256**, 622 (1992).

32. Supported by the Studienstiftung des Deutschen Volkes (J.J.B.) and American Chemical Society Petroleum Research Fund (R.B.). We thank J. Gressier and RioTinto Exploration for samples, the AGSO Isotope & Organic Geochemistry staff for technical assistance, J. Kamprad for x-ray diffraction analyses, T. Blake, D. Des Marais, L. L. Jahnke, C. J. Boreham, D. S. Edwards, T. G. Powell, D. E. Canfield, and M. R. Walter for advice, and J. M. Hayes, A. Knoll, and an anonymous reviewer for their thoughtful comments. G.A.L. and R.E.S. publish with the permission of the Executive Director of AGSO.

19 May 1999; accepted 13 July 1999

REPORTS

Josephson Persistent-Current Qubit

J. E. Mooij,[1,2]* T. P. Orlando,[2] L. Levitov,[3] Lin Tian,[3] Caspar H. van der Wal,[1] Seth Lloyd[4]

A qubit was designed that can be fabricated with conventional electron beam lithography and is suited for integration into a large quantum computer. The qubit consists of a micrometer-sized loop with three or four Josephson junctions; the two qubit states have persistent currents of opposite direction. Quantum superpositions of these states are obtained by pulsed microwave modulation of the enclosed magnetic flux by currents in control lines. A superconducting flux transporter allows for controlled transfer between qubits of the flux that is generated by the persistent currents, leading to entanglement of qubit information.

In a quantum computer, information is stored on quantum variables such as spins, photons, or atoms (*1*–*3*). The elementary unit is a two-state quantum system called a qubit. Computations are performed by the creation of quantum superposition states of the qubits and by controlled entanglement of the information on the qubits. Quantum coherence must be conserved to a high degree during these operations. For a quantum computer to be of practical value, the number of qubits must be at least 10^4. Qubits have been implemented in cavity quantum electrodynamics systems (*4*), ion traps (*5*), and nuclear spins of large numbers of identical molecules (*6*). Quantum coherence is high in these systems, but it seems difficult or impossible to realize the desired high number of interacting qubits. Solid state circuits lend themselves to large-scale integration, but the multitude of quantum degrees of freedom leads in general to short decoherence times. Proposals have been put forward for future implementation of qubits with spins of individual donor atoms in silicon (*7*), with spin states in quantum dots (*8*), and with d-wave superconductors (*9*); the technology for practical realization still needs to be developed.

In superconductors, all electrons are condensed in the same macrosopic quantum state, separated by a gap from the many quasi-particle states. This gap is a measure for the strength of the superconducting effects. Superconductors can be weakly coupled with Josephson tunnel junctions (regions where only a thin oxide separates them). The coupling energy is given by $E_J(1 - \cos \gamma)$, where the Josephson energy E_J is proportional to the gap of the superconductors divided by the normal-state tunnel resistance of the junction and γ is the gauge-invariant phase difference of the order parameters. The current through a Josephson junction is equal to $I_o \sin \gamma$, with $I_o = (2e/\hbar) E_J$, where e is the electron charge and $\hbar$ is Planck's constant divided by 2π. In a Josephson junction circuit with small electrical capacitance, the numbers of excess Cooper pairs on islands n_i, n_j and the phase differences γ_i, γ_j are related as noncommuting conjugate quantum variables (*10*). The Heisenberg uncertainty between phase and charge and the occurrence of quantum superpositions of charges as well as phase excitations (vortexlike fluxoids) have been demonstrated in experiments (*11*). Coherent charge oscillations in a superconducting quantum box have recently been observed (*12*). Qubits for quantum computing based on charge states have been suggested (*13*, *14*). However, in actual practice, fabricated Josephson circuits exhibit a high level of static and dynamic charge noise due to charged impurities. In contrast, the magnetic background is clean and stable. Here, we present the design of a qubit with persistent currents of opposite sign as its basic states. The qubits

[1]Department of Applied Physics and Delft Institute for Microelectronics and Submicron Technologies, Delft University of Technology, Post Office Box 5046, 2600 GA Delft, Netherlands. [2]Department of Electrical Engineering and Computer Science, [3]Department of Physics and Center for Materials Science and Engineering, [4]Department of Mechanical Engineering, Massachusetts Institute of Technology, Cambridge, MA 02139, USA.

*To whom correspondence should be addressed. E-mail: mooij@qt.tn.tudelft.nl

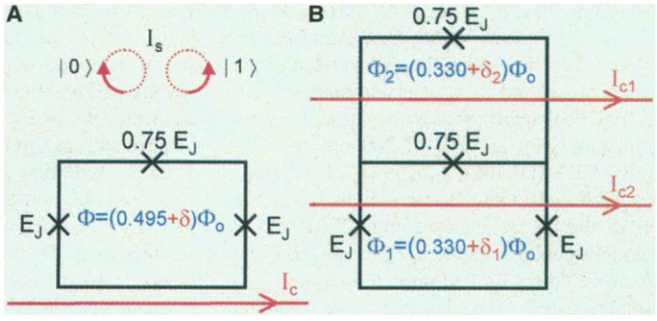

Fig. 1. Persistent current qubit. (**A**) Three-junction qubit. A superconducting loop with three Josephson junctions (indicated with crosses) encloses a flux that is supplied by an external magnet. The flux is $f\Phi_o$, where Φ_o is the superconducting flux quantum and f is 0.495. Two junctions have a Josephson coupling energy E_J, and the third junction has αE_J, where $\alpha = 0.75$. This system has two (meta)stable states |0> and |1> with opposite circulating persistent current. The level splitting is determined by the offset from $\Phi_o/2$ of the flux. The barrier between the states depends on the value of α. The qubit is operated by resonant microwave modulation of the enclosed magnetic flux by a superconducting control line (indicated in red). (**B**) Four-junction qubit. The top junction of (A) is replaced by a parallel junction (SQUID) circuit. There are two loops with equal areas; a magnet supplies a static flux $0.330\Phi_o$ to both. Qubit operations are performed with currents in superconducting control lines (indicated in red) on top of the qubit, separated by a thin insulator. The microwave current I_{c1} couples only to the bottom loop and performs qubit operations as in (A). I_{c2} couples to both loops; it is used for qubit operations with suppressed σ_z action and for an adiabatic increase of the tunnel barrier between qubit states to facilitate the measurement.

can be driven individually by magnetic microwave pulses; measurements can be made with superconducting magnetometers [superconducting quantum interference devices (SQUIDs)]. They are decoupled from charges and electrical signals, and the known sources of decoherence allow for a decoherence time of more than 1 ms. Switching is possible at a rate of 100 MHz. Entanglement is achieved by coupling the flux, which is generated by the persistent current, to a second qubit. The qubits are small (of order 1 μm), can be individually addressed, and can be integrated into large circuits.

Our qubit in principle consists of a loop with three small-capacitance Josephson junctions in series (Fig. 1A) that encloses an applied magnetic flux $f\Phi_o$ (Φ_o is the superconducting flux quantum $h/2e$, where h is Planck's constant); f is slightly smaller than 0.5. Two of the junctions have equal Josephson coupling energy E_J; the coupling in the third junction is αE_J, with $0.5 < \alpha < 1$. Useful values are $f = 0.495$ and $\alpha = 0.75$ (as chosen in Fig. 1A). This system has two stable classical states with persistent circulating currents of opposite sign. For $f = 0.5$, the energies of the two states are the same; the offset from 0.5 determines the level splitting. The barrier for quantum tunneling between the states depends strongly on the value of α. The four-junction version (Fig. 1B) allows modulation of this barrier in situ. Here, the third junction has been converted into a parallel circuit of two junctions, each with a coupling energy αE_J. The four-junction qubit behaves as the three-junction circuit of Fig. 1A, with an enclosed flux $(f_1 + f_2/2)\Phi_o$ and a third-junction (SQUID) strength $2\alpha E_J \cos(f_2\pi)$. The constant fluxes $f\Phi_o$, $f_1\Phi_o$, and $f_2\Phi_o$ are supplied by an external, static, homogeneous magnetic field. Control lines on a separate fabrication level couple inductively to individual qubit loops. All operations on qubits are performed with currents in the control lines.

When γ_1 and γ_2 are the gauge-invariant phase differences across the left and right junctions, the Josephson energy of the four-junction qubit U_J is

$$U_J/E_J = 2 + 2\alpha - \cos\gamma_1 - \cos\gamma_2 - 2\alpha\cos(f_2\pi)\cos(2f_1\pi + f_2\pi + \gamma_1 - \gamma_2) \quad (1)$$

In this expression, the self-generated flux has been neglected. Although this flux will be used for coupling of qubits, it is much smaller than the flux quantum and only slightly changes the picture here. U_J is 2π periodic in γ_1 and γ_2 (Fig. 2A) for the parameter values $\alpha = 0.75$ and $f_1 = f_2 = 0.330$. Each unit cell has two minima L_{ij} and R_{ij} with left- and right-handed circulating currents of about $0.75I_o$ at approximate γ_1,γ_2 values of $\pm 0.27\pi$. The minima would have been symmetric for $2f_1 + f_2 = 1$, which corresponds to a three-junction loop enclosing half a flux quantum. The set of all L minima yields one qubit state and the set of R minima the other. In γ_1,γ_2 space, there are saddle-point connections between L and R minima as indicated with red (intracell, in) and blue lines (intercell, out). Along such trajectories, the system can tunnel between its macroscopic quantum states. The Josephson energy along the trajectories is plotted in Fig. 2B. The saddle-point energies U_{in} and U_{out} depend on α and f_2; lower SQUID coupling gives lower U_{in} but higher U_{out}. For $2\alpha\cos(f_2\pi) < 0.5$, the barrier for intracell tunneling has disappeared, and there is only one minimum with zero circulating current.

Motion of the system in γ_1,γ_2 space can be discussed in analogy with motion of a mass-carrying particle in a landscape with periodic potential energy. Motion in phase space leads to voltages across junctions. The kinetic energy is the associated Coulomb charg-

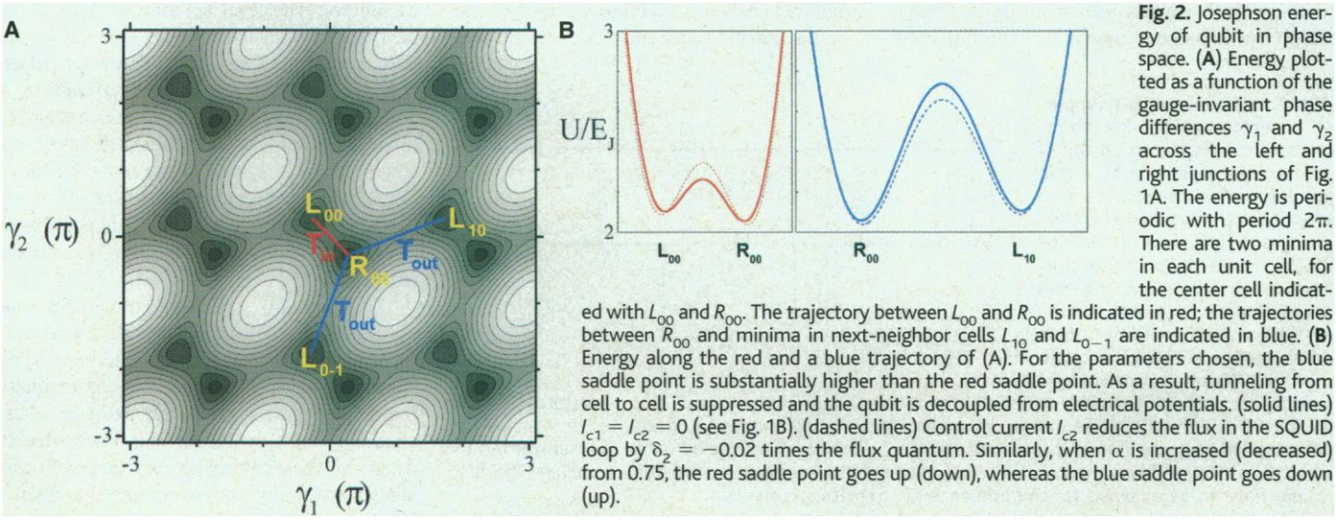

Fig. 2. Josephson energy of qubit in phase space. (**A**) Energy plotted as a function of the gauge-invariant phase differences γ_1 and γ_2 across the left and right junctions of Fig. 1A. The energy is periodic with period 2π. There are two minima in each unit cell, for the center cell indicated with L_{00} and R_{00}. The trajectory between L_{00} and R_{00} is indicated in red; the trajectories between R_{00} and minima in next-neighbor cells L_{10} and L_{0-1} are indicated in blue. (**B**) Energy along the red and a blue trajectory of (A). For the parameters chosen, the blue saddle point is substantially higher than the red saddle point. As a result, tunneling from cell to cell is suppressed and the qubit is decoupled from electrical potentials. (solid lines) $I_{c1} = I_{c2} = 0$ (see Fig. 1B). (dashed lines) Control current I_{c2} reduces the flux in the SQUID loop by $\delta_2 = -0.02$ times the flux quantum. Similarly, when α is increased (decreased) from 0.75, the red saddle point goes up (down), whereas the blue saddle point goes down (up).

ing energy of the junction capacitances. The mass is proportional to the junction capacitance C because other capacitance elements are small. The effective mass tensor has principal values M_a and M_b in the $\gamma_1 - \gamma_2 = 0$ and $\gamma_1 + \gamma_2 = 0$ directions. For the chosen values of the circuit parameters, these principal values are $M_a = \hbar^2/(4E_C)$ and $M_b = \hbar^2/(E_C)$, where the charging energy is defined as $E_C = e^2/2C$. The system will perform plasma oscillations in the potential well with frequencies $\hbar\omega_b \approx 1.3(E_C E_J)^{1/2}$ and $\hbar\omega_a \approx 2.3(E_C E_J)^{1/2}$. The tunneling matrix elements can be estimated by calculation of the action in the Wentzel-Kramers-Brillouin approximation. For tunneling within the unit cell between the minima L and R, the matrix element is $T_{in} \approx \hbar\omega_b \exp[-0.64(E_J/E_C)^{1/2}]$; for tunneling from cell to cell, the matrix element is $T_{out} \approx 1.6\hbar\omega_b \exp[-1.5(E_J/E_C)^{1/2}]$. For the qubit, a subtle balance has to be struck: The plasma frequency must be small enough relative to the barrier height to have well-defined states with a measurable circulating current but large enough (small enough mass) to have substantial tunneling. The preceding qualitative discussion has been confirmed by detailed quantitative calculations in phase space and in charge space (*15*). From these calculations, the best parameters for qubits can be determined. In practice, it is possible to controllably fabricate aluminum tunnel junctions with chosen E_J and E_C values in a useful range.

It is strongly desirable to suppress the intercell tunneling T_{out}. This suppression leads to independence from electrical potentials, even if the charges on the islands are conjugate quantum variables to the phases. The qubit system in phase space is then comparable to a crystal in real space with nonoverlapping atomic wave functions. In such a crystal, the electronic wave functions are independent of momentum; similarly, charge has no influence in our qubit.

Mesoscopic aluminum junctions can be reliably fabricated by shadow evaporation with critical current densities up to 500 A/cm^2. In practice, a junction of 100 nm^2 by 100 nm^2 has E_J around 25 GHz and E_C around 20 GHz. A higher E_J/E_C ratio can be obtained by increasing the area to which E_J is proportional and E_C is inversely proportional. A practical qubit would, for example, have junctions with an area of 200 nm^2 by 400 nm^2, $E_J \sim 200$ GHz, $E_J/E_c \sim 80$, level splitting $\Delta E \sim 10$ GHz, barrier height around 35 GHz, plasma frequency around 25 GHz, and tunneling matrix element $T_{in} \sim 1$ GHz. The matrix element for undesired tunneling T_{out} is smaller than 1 MHz. The qubit size would be of order 1 μm; with an estimated inductance of 5 pH, the flux generated by the persistent currents is about $10^{-3}\Phi_o$.

To calculate the dependence of the level splitting on f_1 and f_2, we apply a linearized approximation in the vicinity of $f_1 = f_2 = 1/3$, defining F as the change of U_J away from the minimum of $U_J(\gamma_1,\gamma_2)$. This yields $F/E_J = 1.2[2(f_1 - 1/3)+(f_2 - 1/3)]$. The level splitting without tunneling would be $2F$. With tunneling, symmetric and antisymmetric combinations are created; the level splitting is now $\Delta E = 2(F^2 + T_{in}^2)^{1/2}$. As long as $F \gg T_{in}$, the newly formed eigenstates are localized in the minima of $U_J(\gamma_1,\gamma_2)$.

We discuss qubit operations for the four-junction qubit. They are driven by the currents I_{ca} and I_{cb} in the two control lines (Fig. 1B). The fluxes induced in the two loops, normalized to the flux quantum, are $\delta_1 = (L_{a1}I_{ca} + L_{b1}I_{cb})/\Phi_o$ and $\delta_2 = (L_{a2}I_{ca} + L_{b2}I_{cb})/\Phi_o$. The control line positions are chosen such that $L_{a2} = 0$ and $L_{b2} = -2L_{b1}$. When the two loops have equal areas, $f_1 = f_2$ for zero control current. We assume that the qubit states are defined with zero control current and that δ_1 and δ_2 act as perturbations to this system. The effective Hamiltonian operator (H_{op}) in terms of Pauli spin matrices σ_x and σ_z for the chosen parameters is about

$$H_{op}/\Delta E \approx (80\delta_1 + 42\delta_2)\sigma_z - (9.2\delta_1 + 8.3\delta_2)\sigma_x \quad (2)$$

The numerical prefactors follow from the variational analysis of the influence of δ_1 and δ_2 on the tunnel barrier and the level splitting.

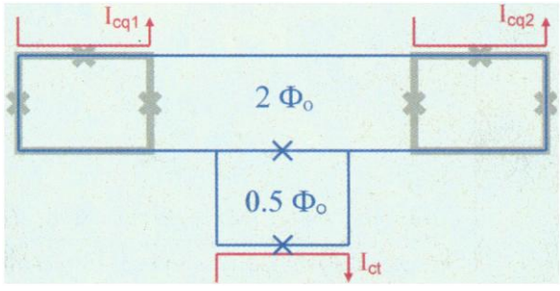

Fig. 3. Switchable qubit coupler. A superconducting flux transporter (blue) is placed on top of two qubits, separated by a thin insulator. The transporter is a closed loop that contains two Josephson junctions in parallel (SQUID) with high critical current. In the off state, the two loops of the transporter contain an integer number of flux quanta (main loop) and half a flux quantum (SQUID loop), supplied by a permanent magnet. The current response to a flux change is very small. In the on state, the flux in the SQUID loop is made integer by means of a control current I_{ct} (red). As the transporter attempts to keep the flux in its loop constant, a flux change induced by qubit 1 is transmitted to qubit 2. As shown here, the two three-junction qubits experience $\sigma_z \otimes \sigma_z$-type coupling. The flux values have to be adjusted for the influence of circulating currents.

The terms that contain σ_x can be used to induce Rabi oscillations between the two states, applying microwave pulses of frequency $\Delta E/h$. There are two main options, connected to one of the two control lines. Control current I_{ca} changes δ_1, which leads to a Rabi oscillation (σ_x term) as well as a strong modulation of the Larmor precession (σ_z term). As long as the Rabi frequency is far enough below the Larmor frequency, this is no problem. For $\delta_1 = 0.001$, the Rabi frequency is 100 MHz. This mode is the only one available for the three-junction qubit and is most effective near the symmetry point $f = 0.5$ or $f_1 = f_2 = 1/3$. Control current I_{cb} is used to modulate the tunnel barrier. Here, the σ_z action is suppressed by means of the choice $L_{b2}/L_{b1} = \delta_2/\delta_1 = -2$. However, a detailed analysis shows that with δ_2 modulation, it is easy to excite the plasma oscillation with frequency ω_b. One has to restrict δ_2 to remain within the two-level system. Values of 0.001 for δ_1 or δ_2 correspond to about 50-pW microwave power at 10 GHz in the control line. These numbers are well within practical range.

Two or more qubits can be coupled by means of the flux that the circulating persistent current generates. The current is about 0.3 μA, the self-inductance of the loop is about 5 pH, and the generated flux is about $10^{-3}\Phi_o$. When a superconducting closed loop (a flux transporter) with high critical current is placed on top of both qubits, the total enclosed flux is constant. A flux change $\Delta\Phi$ that is induced by a reversal of the current in one qubit leads to a change of about $\Delta\Phi/2$ in the flux that is enclosed by the other qubit. One can choose to couple the flux, generated in the main loop of qubit 1, to the main loop of qubit 2 ($\sigma_z \otimes \sigma_z$ coupling) or to the SQUID loop of qubit 2 ($\sigma_z \otimes \sigma_x$ coupling). A two-qubit gate operation is about as efficient as a single qubit operation driven with $\delta_1 = 0.001$. An example of a possible controlled-NOT operation with fixed coupling runs as follows: The level splitting of qubit 2 depends on the state of qubit 1, the values are ΔE_{20} and ΔE_{21}. When Rabi microwave pulses, resonant with ΔE_{21}, are applied to qubit 2, it will only react if qubit 1 is in its I1> state. In principle, qubits can be coupled at larger distances. An array scheme as proposed by Lloyd (*1*, *3*), where only nearest neighbor qubits are coupled, is also very feasible. It is possible to create a flux transporter that has to be switched on by a control current (Fig. 3).

The typical switching times for our qubit are 10 to 100 ns. To yield a practical quantum computer, the decoherence time should be at least 100 μs. We can estimate the influence of known sources of decoherence for our system, but it is impossible to determine the real decoherence time with certainty, except by measurement. We discuss

some decohering influences here. All quasiparticle states in the superconductor have to remain unoccupied. In equilibrium, the number is far below 1 at temperatures below 30 mK. Extreme care must be taken to shield the sample from photons. Even 4 K blackbody photons have enough energy to break a Cooper pair. Adequate shielding is possible on the time scale of our computer. Inductive coupling to bodies of normal metal has to be avoided. By decoupling the qubit from electrical potentials, we have eliminated coupling to charged defects in substrate or tunnel barriers. The aluminum nuclei have a spin that is not polarized by the small magnetic fields at our temperature of 25 mK. Statistical fluctuations will occur, but their time constant is very long because of the absence of electronic quasi-particles. The net effect will be a small static offset of the level splitting, within the scale of the variations due to fabrication. The dephasing time that results from unintended dipole-dipole coupling of qubits is longer than 1 ms if the qubits are farther apart than 1 μm. Emission of photons is negligible for the small loop. Overall, the sources of decoherence that we know allow for a decoherence time above 1 ms.

Requirements for a quantum computer are that the qubits can be prepared in well-defined states before the start of the computation and that their states can be measured at the end. Initialization will proceed by cooling the computer to below 50 mK and having the qubits settle in the ground state. For the measurement, a generated flux of $10^{-3}\Phi_o$ in an individual qubit can be detected with a SQUID if enough measuring time is available. A good SQUID has a sensitivity of $10^{-5}\Phi_o/\mathrm{Hz}^{1/2}$, so that a time of 100 μs is required. Usual SQUIDs have junctions that are shunted with normal metal. The shunt introduces severe decoherence in a qubit when the SQUID is in place, even if no measurement is performed. We are developing a nonshunted SQUID that detects its critical current by discontinuous switching. For a measurement at the end of a quantum computation scheme, the qubit can be frozen by an adiabatic increase of the tunnel barrier between the two qubit states. As Fig. 2 indicates, we can increase the barrier by a change of control current. A similar procedure, as suggested by Shnirman and Schön (*14*), for charge qubits can be followed.

The proposed qubit should be of considerable interest for fundamental studies of macroscopic quantum coherence, apart from its quantum computing potential. Compared with the radio frequency SQUID systems that have been used in attempts to observe such effects (*16*) and also have been suggested as possible qubits for quantum computation (*17*), the much smaller size of the qubit decouples it substantially better from the environment.

References and Notes

1. S. Lloyd, *Science* **261**, 1569 (1993).
2. C. H. Bennett, *Phys. Today* **48** (no. 10), 24 (1995); D. P. DiVincenzo, *Science* **270**, 255 (1995); T. P. Spiller, *Proc. IEEE* **84**, 1719 (1996).
3. S. Lloyd, *Sci. Am.* **273** (no. 4), 140 (1995).
4. Q. A. Turchette, C. J. Hood, W. Lange, H. Mabuchi, H. J. Kimble, *Phys. Rev. Lett.* **75**, 4710 (1995).
5. C. Monroe, D. M. Meekhof, B. E. King, W. M. Itano, D. J. Wineland, *ibid.*, p. 4714.
6. N. A. Gershenfeld and I. L. Chuang, *Science* **275**, 350 (1997).
7. B. Kane, *Nature* **393**, 133 (1998).
8. D. Loss and D. DiVincenzo, *Phys. Rev. A* **57**, 120 (1998).
9. L. B. Ioffe, V. B. Geshkenbein, M. V. Feigel'man, A. L. Fauchère, G. Blatter, *Nature* **398**, 679 (1999).
10. D. V. Averin and K. K. Likharev, in *Mesoscopic Phenomena in Solids*, B. L. Altshuler, P. A. Lee, R. A. Webb, Eds. (North Holland, Amsterdam, 1991), pp. 173–271.
11. W. J. Elion, M. Matters, U. Geigenmuller, J. E. Mooij, *Nature* **371**, 594 (1994); L. S. Kuzmin and D. B. Haviland, *Phys. Rev. Lett.* **67**, 2890 (1991); P. Joyez, D. Esteve, M. H. Devoret, *ibid.* **80**, 1956 (1998).
12. Y. Nakamura, Yu. A. Pashkin, J. S. Tsai, *Nature* **398**, 786 (1999).
13. A. Shnirman, G. Schön, Z. Hermon, *Phys. Rev. Lett.* **79**, 2371 (1997); D. V. Averin, *Solid State Commun.* **105**, 659 (1998); Yu. Makhlin, G. Schön, A. Shnirman, *Nature* **398**, 305 (1999).
14. A. Shnirman and G. Schön, *Phys. Rev. B* **57**, 15400 (1998).
15. T. P. Orlando *et al.*, in preparation.
16. C. D. Tesche, *Phys. Rev. Lett.* **64**, 2358 (1990); R. Rouse, S. Han, J. E. Lukens, *ibid.* **75**, 1614 (1995).
17. M. F. Bocko, A. M. Herr, M. J. Feldman, *IEEE Trans. Appl. Supercond.* **7**, 3638 (1997).

18. We thank J. J. Mazo, C. J. P. M. Harmans, A. C. Wallast, and H. Tanaka for important discussions. This work is partially supported by Army Research Office grant DAAG55-98-1-0369, Stichting voor Fundamenteel Onderzoek der Materie, NSF Award 67436000IRG, and the New Energy and Industrial Technology Development Organization.

22 April 1999; accepted 7 July 1999

Energetic Iron(VI) Chemistry: The Super-Iron Battery

Stuart Licht,* Baohui Wang, Susanta Ghosh

Higher capacity batteries based on an unusual stabilized iron(VI) chemistry are presented. The storage capacities of alkaline and metal hydride batteries are largely cathode limited, and both use a potassium hydroxide electrolyte. The new batteries are compatible with the alkaline and metal hydride battery anodes but have higher cathode capacity and are based on available, benign materials. Iron(VI/III) cathodes can use low-solubility K_2FeO_4 and $BaFeO_4$ salts with respective capacities of 406 and 313 milliampere-hours per gram. Super-iron batteries have a 50 percent energy advantage compared to conventional alkaline batteries. A cell with an iron(VI) cathode and a metal hydride anode is significantly (75 percent) rechargeable.

Improved batteries are needed for various applications such as consumer electronics, communications devices, medical implants, and transportation needs. The search for higher capacity electrochemical storage has focused on a wide range of materials, such as carbonaceous materials (*1*), tin oxide (*2*), grouped electrocatalysts (*3*), or macroporous minerals (*4*). Of growing importance are rechargeable (secondary) batteries such as metal hydride (MH) batteries (*5*), which this year have increased the commercial electric car range to 250 km per charge. In consumer electronics, primary, rather than secondary, batteries dominate. Capacity, power, cost, and safety factors have led to the annual global use of approximately 6×10^{10} alkaline or dry batteries, which use electrochemical storage based on a Zn anode, an aqueous electrolyte, and a MnO_2 cathode, and which constitute the vast majority of consumer batteries. Despite the need for safe, inexpensive, higher capacity electrical storage, the aqueous MnO_2/Zn battery has been a dominant primary battery chemistry for over a century. Contemporary alkaline and MH batteries have two common features: Their storage capacity is largely cathode limited and both use a KOH electrolyte.

We report a new class of batteries, referred to as super-iron batteries, which contain a cathode that uses a common material (Fe) but in an unusual (greater than 3) valence state. Although they contain the same Zn anode and electrolyte as conventional alkaline batteries, the super-iron batteries provide >50% more energy capacity. In addition, the Fe(VI) chemistry is rechargeable, is based on abundant starting materials, has a relatively environmentally benign discharge product, and appears to be compatible with the anode of either the primary alkaline or secondary MH batteries.

The fundamentals of MnO_2 chemistry continue to be of widespread interest (*6*). The storage capacity of the aqueous MnO_2/Zn

Department of Chemistry and Institute of Catalysis Science, Technion—Israel Institute of Technology, Haifa 32000, Israel.

*To whom correspondence should be addressed. E-mail: chrlicht@techunix.technion.ac.il